Journal of Materials Science & Nanotechnology
Volume 8 | Issue 1
ISSN: 2348-9812

Research Article Open Access

Effect of Raw Materials and Mechanical Alloying on $W_{50}Ti_{50}$ Alloy Fabrication

Wang QX[1,2], Chen H[*1] and Cui GD[1]

[1]School of Materials Science and Engineering, Southwest Jiaotong University, Chengdu, China
[2]Sino-Euro Materials Technologies of Xi'an Co., Ltd. Xi'an, China

[*]**Corresponding author:** Chen H, School of Materials Science and Engineering, Southwest Jiaotong University, Chengdu, 610031, China, Tel: +86 29 89165488, E-mail: 43550577@qq.com

Citation: Wang QX, Chen H, Cui GD (2020) Effect of Raw Materials and Mechanical Alloying on $W_{50}Ti_{50}$ Alloy Fabrication. J Mater Sci Nanotechnol 8(1): 101

Received Date: March 12, 2020 Accepted Date: December 21, 2020 Published Date: December 23, 2020

Abstract

W-Ti solid solution powders were prepared by mechanical alloying for 60 h and annealing at 500 °C for 30 min with W-TiH_2 mixed powders and W-Ti mixed powders respectively. The $W_{50}Ti_{50}$ alloy were then compacted into cylindrical samples followed by sintering at 1400 °C for 2 h. The results show that TiH_2 phases decomposed and the new phases of TiH and W-Ti solid solution were obtained after milling for 60 h. Moreover, irregular nanoroads of W-TiH_2 solid solution with the diameter range of 10~30 nm was prepared during the isothermal annealing process. The hydrogen contents of the W-TiH_2 starting powders, MA powders, annealed powders and alloy are 4200 ppm, 1350 ppm, 8 ppm and 9ppm, respectively. The $W_{50}Ti_{50}$ solid solution was obtained with W-TiH_2 milled powders. The relative density, Vickers hardness and electrical resistivity of $W_{50}Ti_{50}$ alloy with W-TiH_2 milling powders were 98.3%~99.2%, 546Hv and 7.18μΩ-cm, respectively. The sequence of phase transformations during those processes was also proposed.

Keywords: Tungsten; Titanium; TEM; $W_{50}Ti_{50}$ Solid Solution; Nanoroads

Introduction

In the 1970s, the mechanical alloying (MA) process was found by Benjamin *et al.* [1,2], which is now accepted as a versatile technique for obtaining oxide-dispersion -strengthened superalloys [1], intermetallic compounds [3,4], supersaturated solid solutions [5] and amorphous phases [6], among others materials. The transformation which control the stages of the initial elements into final phases during the mechanical alloying process are not still clear. Crucially, though, previous works [7,8] have showed that the transformation stages could depend on the chemical composition and MA conditions.

W-Ti-(N/O) film prepared by W-Ti alloy with 10~30wt.%Ti were often applied to in microelectronic device manufacture as diffusion barriers between copper and silicon layers [9-11]. Normally, the W-10~30wt.%Ti alloy was prepared with simplex (W and Ti powders) or prealloy powders by PM method such as HP [12], SPS [13,14] and HIP [15]. Moreover, the soft chemical approach (SCA) was also used to obtain nanostructured W-10~20wt.%Ti alloys [16]. Moreover, it has been found that the powder structure and properties had obvious effect on the W-Ti alloy [17]. The mechanical alloying was used to obtain W-Ti prealloy powders. On one hand, mechanical alloying can vary the solubility between Ti and W during. On the other hand, different phase evolution was obtained during the annealing process with the ball-milled powders. That variation is hoped to affect the solubility of the W-Ti alloy. There are less reports about the preparation of W-Ti solid solution powders and alloy. We tried to synthesize nanoroads of W-Ti solid solution through balling milling and isothermal annealing, and then the alloy was prepared by sintered with low temperature. The preparation principle of $W_{50}Ti_{50}$ solid solution prepared by W-Ti and W-TiH_2 MA powders was also discussed.

Experimental Section

Powders of 22wt% TiH_2 (99.9%, 50~55 μm), Ti (99.9%, 45~55 μm), and 78 wt% W (99.9%, 6~8 μm) were used as raw materials. W-TiH_2 mixed powders and W-Ti mixed powders were used to prepare for solid solution respectively. The mechanical alloying process was done by the planetary machine with tungsten balls in the nylon containers. The weight ratio of 40:1 was used between W ball and the mixed powder. It was operated at 200 revolutions per minute for 60 h. The milled samples were then annealed at 500 °C for 30 min with Ar atmosphere and the heating rate is 100 °C/min. And then the powders were sintered at 1400 °C for 2h in a hot press furnace with the heating rate of 20-25 °C/min under Ar atmosphere.

The obtained powders and alloy were analyzed by FESEM , TEM (JEOL JEM -3010,200 kV), and EDS. XRD patterns of the powders and alloy were got on a Japan Rigaku D/Max-IIIC diffractometer (40 kV ,40mA , Cu Kα radiation (λ=1.5406 Å)),employing a scanning rate of 8° min^{-1} in the 2θ ranging from 20° to 80°. Drainage method was used to test the density of the alloy samples.

Moreover, the hardness and resistivity of sintered samples were determined by Vickers hardness tester (Leica VM) and four probe technique (RTS-8) respectively.

Results and Analysis

Figure 1 presents the XRD patterns of W-TiH_2 and W-Ti powders. As seen from Figure 1a and b, there are bcc W (JCPDS No.04-0806) and fcc TiH_2 (JCPDS No. 65-0708) phases in the starting material. However, after milled for 60 h, the fcc TiH_2 phases disappeared while a new phase of fcc TiH (JCPDS No. 40-1244) with FWHM (111) was obtained. Moreover, the FWHMs (110), (211), (220) of W increase and those peaks shift to the left a little which is due to the rapid crystallite refinement and the formation of a W-Ti solid solution. When the milled powders were annealed at 500 °C for 30min, the (111) peak of fcc TiH disappeared and only β (W/Ti) solid solution (JCPDS No. 49-1440) was obtained as seen in Figure 1c. In addition, no other peaks for impurities were observed. It can be seen from Figure 1d that there are bcc W (JCPDS No.04-0806) and fcc Ti (JCPDS No. 65-3362) phases in the raw material. After MA for 60 h and dealing at 500 °C for 30min, β (W/Ti) solid solution (JCPDS No. 49-1440) appeared while the hcp Ti (002) (JCPDS No. 65-3362) peak did not disappeared as seen in Figure 1e and f. The surface of Ti powders is easily oxidized which can reduce the solution between element of W and Ti.

After the MA process, the crystallite size of pre-alloyed powder decreases rapidly. Moreover, X-ray diffraction spectrum widening can be used to estimate the crystallite size and macrostrain of powders when the crystallite diameters were less than 200 nm. Therefore, Scherer's formula can be used to estimate the effective crystallite size and macrostrain of powder particles. The crystallite size and lattice distortion of the powder are calculated by using the Voigt function single-peak analysis method after eliminating the widening caused by the instrument, and the full width at half maximum and integral width of the diffraction peak of the β (W/Ti) (110) plane. In this study, the Voigt function unimodal analysis method was used to strip the geometric widening, to separate the widening caused by crystallite size and lattice distortion. Voigt function can be regarded as the convolution of Gaussian function and Cauchy function, and h (x) and g (x) can also be regarded as the convolution of Gaussian and Cauchy components respectively. Gaussian component and Cauchy component widening effect can be separated by the ratio Φ between the full width at half maximum 2m and the integral width β, i.e. the Voigt parameter. When Φ = 0.63662, the peak shape is a full Cauchy distribution. When Φ = 0.93949, it is a full Gaussian distribution. When 0.63662 <Φ <0.93949, the Gauss component integral width β_G and Cauchy component integral width βc can be divided by the following half Empirical formula 1.1 and 1.2.

$$\beta_C/\beta = 2.0207 - 0.4803\Phi - 1.7756\Phi^2 \quad (1.1)$$

$$\beta_G/\beta = 0.6420 + 1.4187(\Phi - 0.6366)^{0.5} - 2.2043\Phi + 1.8706\Phi^2 \quad (1.2)$$

If superscripts h, g, and f are used to represent the experimental line type, instrument line type, and sample eigenline type, respectively, and the subscripts G and C are Gaussian and Cauchy components, respectively, the following relationship exists between the three integral widths p:

$$\beta_C^f = \beta_C^h - \beta_C^g \quad (1.3)$$

$$(\beta_C^f)^2 = (\beta_C^h)^2 - (\beta_C^g)^2 \quad (1.4)$$

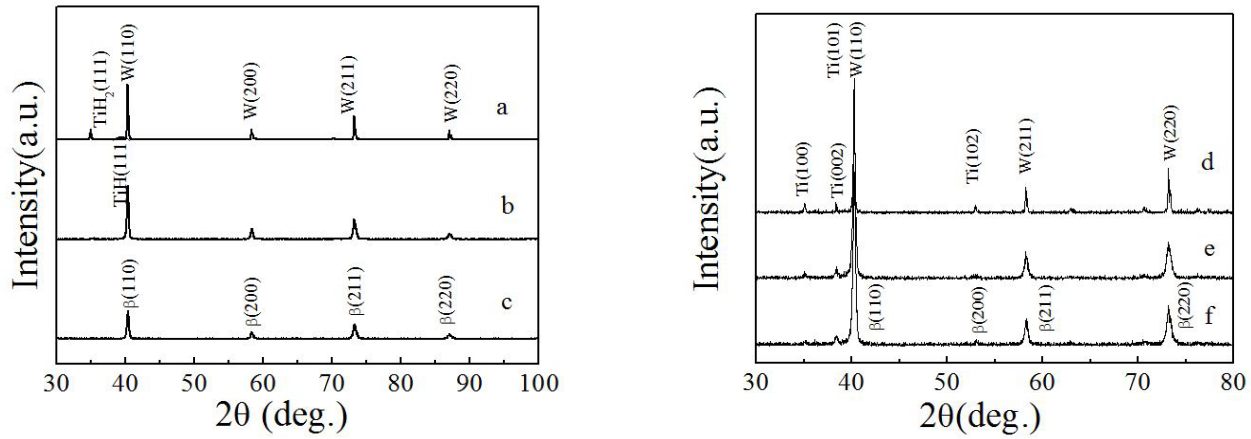

Figure 1: X-ray diffraction patterns of samples **(a)** W-TiH_2 starting material; **(b)** W-TiH_2 powders milled for 60 h; **(c)** W-TiH_2 milled powders annealed at 500 °C; **(d)** W-Ti starting material; **(e)** W-Ti powders milled for 60 h; **(f)** W-Ti milled powders annealed at 500 °C

Therefore, after obtaining the FWHM and integral width of the peak shape of the instrument and the experimental peak shape, the integral width reflecting the crystallite size characteristics of the sample and the integral width caused by lattice distortion can be obtained from the formula, and the integral width of the crystallite size characteristics, which is βr in the Scherer formula. According to the above formula, the crystallite size and micro strain of the diffraction peaks of the β(W/Ti) (110) plane were calculated using the FWHM and the integrated width of the peaks. The results show that the crystallite size and micro strain for the W-Ti powders was 30-35 nm and 0.22%, respectively Moreover, the crystallite size and micro strain for the W-Ti powders was 27-32 nm and 0.20%, respectively.

The microstructure of powders was obtained by TEM and SEAD as seen in Figure 2. The powder size is small but agglomerate is serious (Figure 2a and b). When the MA powder was annealed, there are a lot of irregular nanoroads with the diameter range of 10~30 nm was obtained. Moreover, energy dispersive spectrometer was used to measure the chemical composition of the powders which is seen in Figure 2c. The nanoroads were composed of W and Ti elements with the number of atoms W:Ti about 1:1. The Cu-related peaks was due to the presence of Cu grids for testing. To confirm the constituent of β(W/Ti) solution, irregular nanoroads were analyzed by HRTEM as shown in Figure 2d. The crystal plane spacing is about 0.22 nm, 0.16 and 0.13 nm, corresponding to the (110), (200) and (211) crystal planes of β(W/Ti).

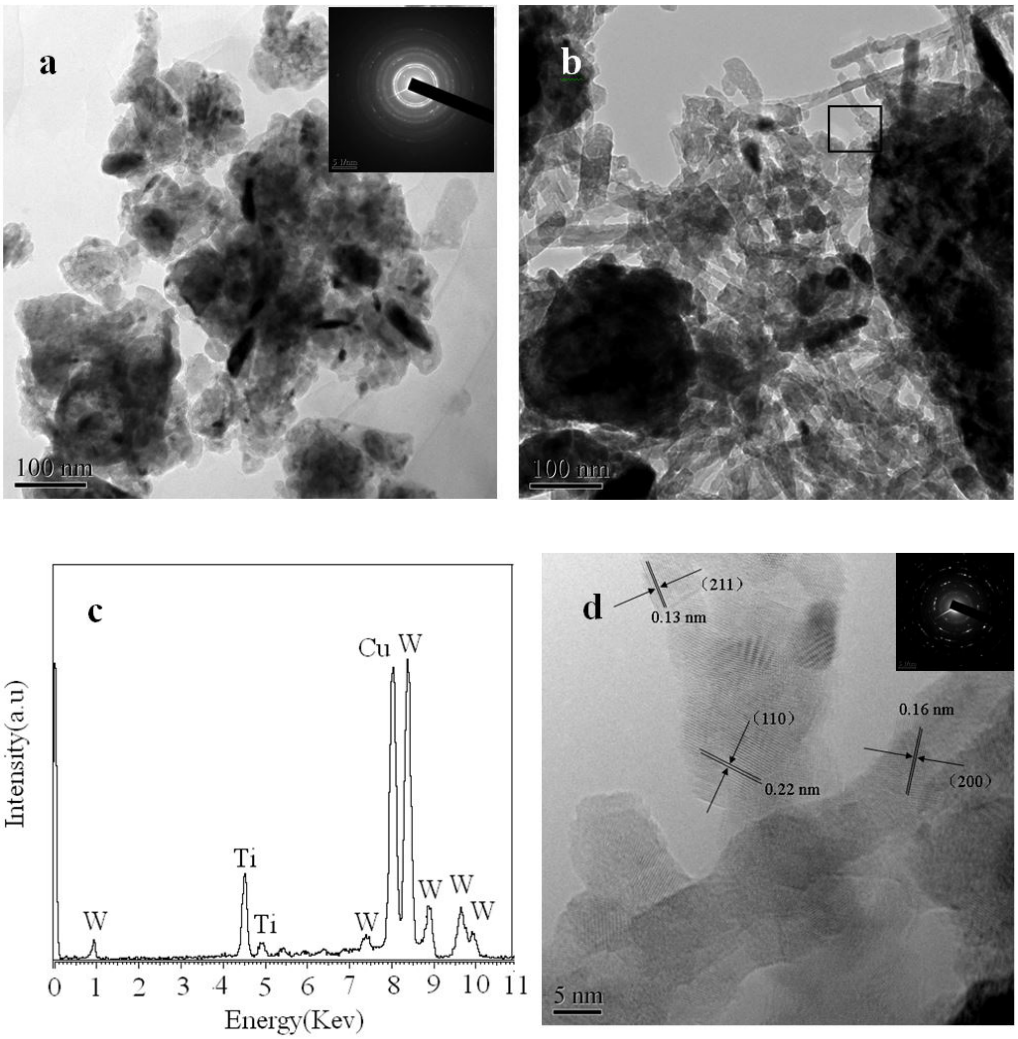

Figure 2: Images of powders **(a)** TEM image of W-Ti powders annealed at 500 °C; **(b)** W-TiH_2 TEM image of MA powders annealed at 500 °C; **(c)** W-TiH_2 EDS; **(d)** W-TiH_2 HRTEM

SEM images of W-Ti, W-TiH_2 powders and alloys are shown in Figure 3. Ti powders are irregular about 44 μm and W powders are quasi-sphere about 6~8 μm as seen from Figure 3a. The sizes of such particles were greatly decreased after MA under the ball-powder-ball collisions and began to agglomerate, fine grey regions and white regions interlacing in the microstructure (Figure 3b,c and d) shows that TiH_2 powders are irregular about 52 μm and W powders are quasi-sphere about 6~8 μm. After milling the mixed powders were smaller than that of W-Ti powders as shown in Figure 3e.

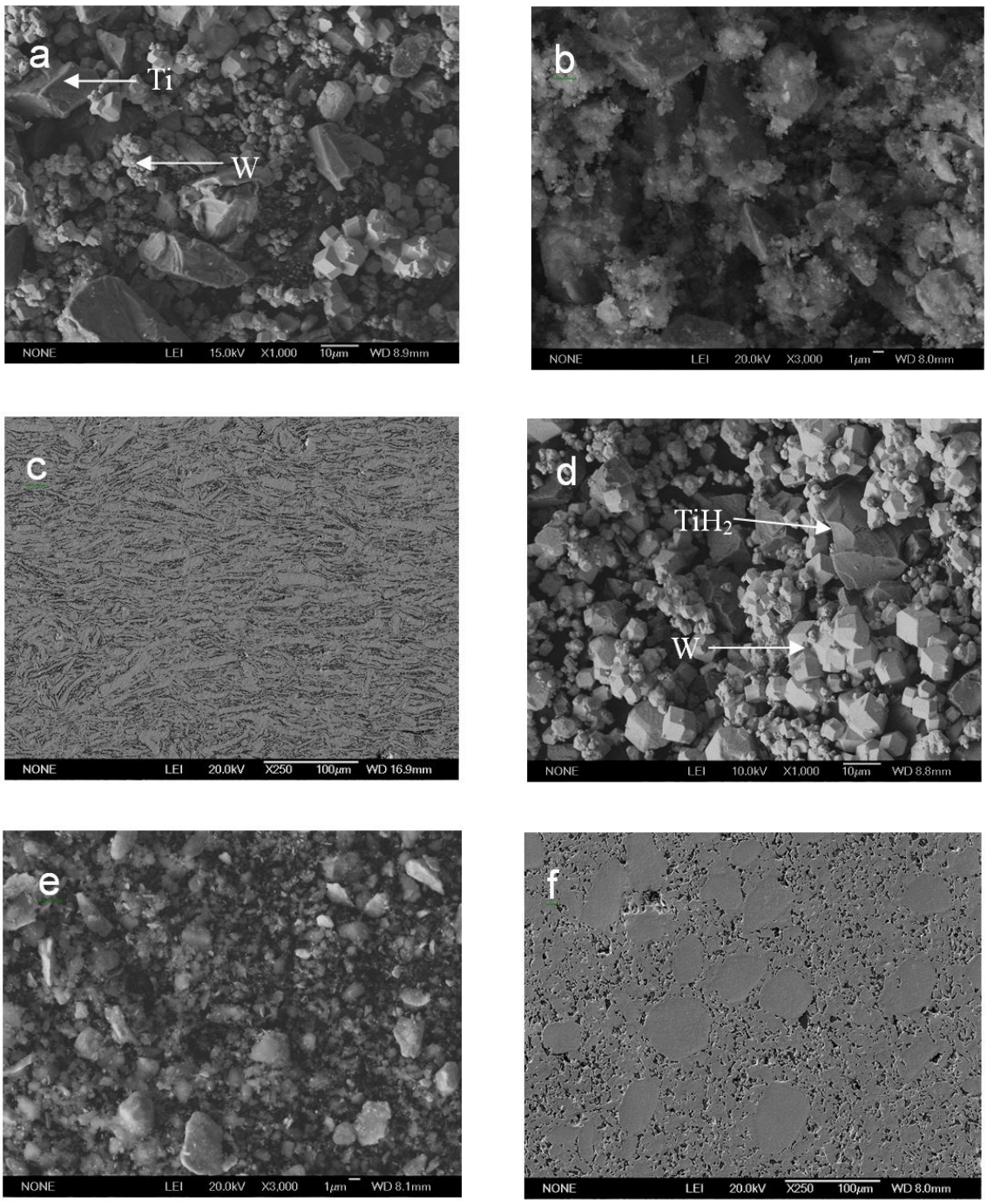

Figure 3: SEM of W-Ti and W-TiH_2 powders and alloys **(a)** W-Ti raw material powders; **(b)** W-Ti milled powders annealed at 500 °C; **(c)** W-Ti alloy prepared by W-Ti MA powders; **(d)** W-TiH_2 raw material powders; **(e)** W-TiH_2 milled powders annealed at 500 °C h; **(f)** W-Ti alloy prepared by W-TiH_2 MA powders

The microstructure of W-Ti alloys obtained by W-Ti and W-TiH_2 milled powders are seen in Figure 3c and Figure 3f. For the W-Ti milled powders in Figure 3c, the dark region is a-Ti and the light region is β(W/Ti) solid solution, respectively which was indicated by XRD patterns as shown in Figure 4a. For the W-TiH2 milled powders in Figure 3f, the dark and light regions are all β(W/Ti) solid solution which was indicated by XRD patterns as shown in Figure 4b. Moreover, the dark region of β(W/Ti) solid solution is mainly the Ti matrix(Ti_xW_{1-x}) while the light region is W matrix(W_xTi_{1-x}). EDS analysis (Figure 5) was used to confirm the compositions. It can be seen that after the sintering process, the composition of W and Ti elements prepared by W-Ti powders is nonuniform as seen in Figure 5a. The pure Ti are found which proved by XRD patterns as shown in Figure 4a. However, the composition of W and Ti elements prepared by W-TiH_2 powders is uniform as seen in Figure 5b which indicated that the $W_{50}Ti_{50}$ solid solution were obtained.

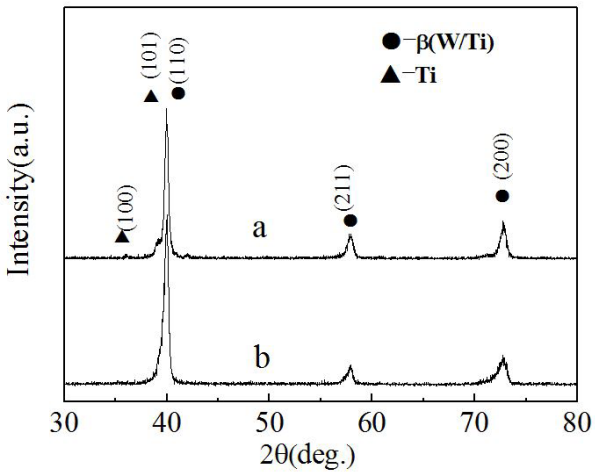

Figure 4: X-ray diffraction patterns of samples **(a)** W-Ti alloy obtained by W-Ti MA powders; **(b)** W-Ti alloy obtained by W-TiH_2 MA powders

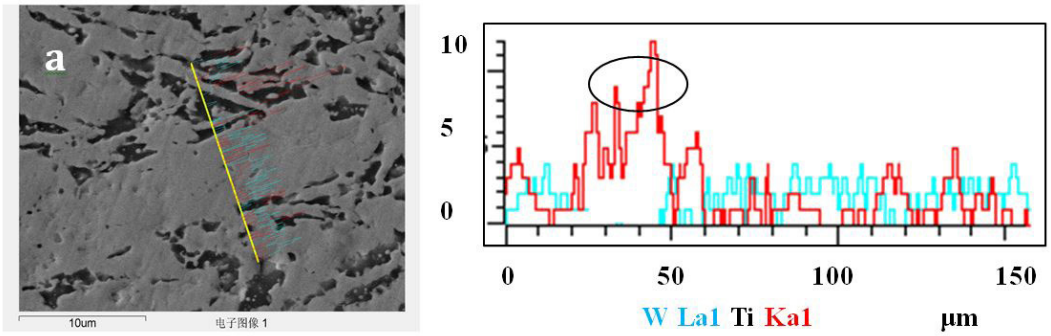

Figure 5: EDS analyze of samples **(a)** W-Ti alloy obtained by W-Ti MA powders; **(b)** W-Ti alloy prepared by W-TiH_2 MA powders

By verifying whether these elements are truly alloyed, the hydrogen contents of the samples were analyzed by chemical method. The hydrogen contents of the W-TiH_2 starting powders, MA powders, annealed powders and alloys is 4200 ppm, 1350 ppm, 8 ppm, 9 ppm respectively. It suggests that TiH_2 powders were partly decomposed in the course of the MA process and completely decomposed after annealing process, which is corresponding to the XRD results. The decomposition of W-TiH_2 powders occurs during 499 °C to 543 °C. While the decomposition of W-TiH_2 milled powders happens during 396 °C to 427 °C, which indicates that the decomposition temperature was decreased after the milling process. The finer particle of W-TiH_2 can shorten the diffusion path between Ti and W, which can increase the W-Ti solid solution formation. Because active Ti atoms decomposed from TiH_2 easily diffuses into W matrix to form W-Ti solid solution. Therefore, W-TiH_2 milled powders as an additive of Ti elements is better for W-Ti alloy.

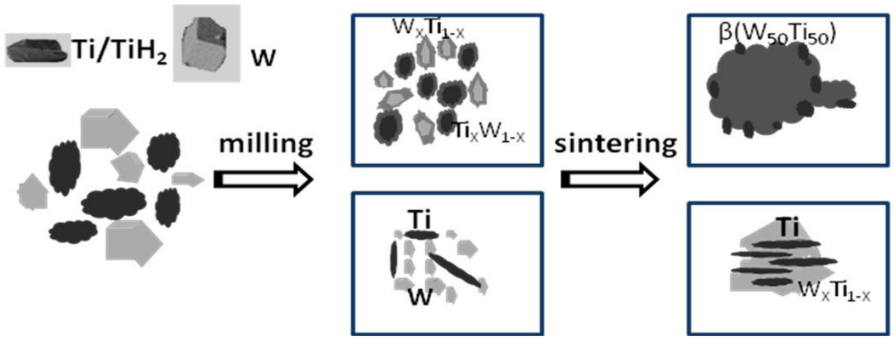

Figure 6: Schematic of $W_{50}Ti_{50}$ solid solution prepared by W-Ti and W-TiH_2 MA powders

The sequence of phase transformations of $W_{50}Ti_{50}$ solid solution during the mechanical alloying, isothermal annealing and sintering can be schematically described as Figure 6. For the W-Ti powders, it is known that Ti was easily oxidation to a thin film on the surface of the powders and it is soft enough to be out of shape. After milling, the Ti powders were mostly laminar structure. During the compacting and sintering, the laminar structure of Ti was retained as seen in Figure 3C. Only the size of W powder was smaller diffused by Ti atoms to form the W_xTi_{1-x} solid solution. When the TiH_2 particles and W particles (6-8μm) were mixed and milled, the size of both powders is smaller and smaller, during the milling, annealing and sintering process the Ti matrix (Ti_xW_{1-x}) and W matrix (W_xTi_{1-x}) solid solutions were obtained.

Moreover, as the milled powders were annealing and compacting, the particles would fill the gap between each other. Additionally, the nanoparticles exhibit good sintering performance [9]. Alloys with high relative density can be prepared with high energy milling at lower sintering temperatures. The MA powders were nanoparticles which exhibit better sintering performance. Moreover, the active Ti atoms also accelerate the formation of W-Ti solid solution. It certainly increases the binding properties. After the deeply diffusion between W and Ti atom the $W_{50}Ti_{50}$ solid solutions can be generated.

The relative densities of W-Ti alloys sintered with W-Ti and W-TiH_2 milled powders varied between 97.1-97.9% and 98.3%~99.2%, respectively. The Vickers hardness and resistivity data of W-Ti alloy with W-Ti and W-TiH2 milled powders were different. Vickers hardness of 605±150 Hv, and 555±15 Hv are achieved in W-Ti alloy with the different powders. For the W-Ti milled powders, the range of hardness values is uneven because of the a-Ti and the β(W/Ti) solid solution. Moreover, the resistivity data for W-Ti alloys sintered with W-Ti and W-TiH_2 milled powders was 8.36μΩ-cm and 7.18μΩ-cm, respectively, which is described to higher resistivity of Ti compared to W [16-19].

Conclusion

We successfully synthesized the $W_{50}Ti_{50}$ solid solution with W-TiH_2 milled powders. During the process irregular nanoroads of W-Ti solid solution with diameter range of 10~30 nm through MA for 60 h and isothermal heat treatment at 500 °C for 30 min. Not only W matrix (W_xTi_{1-x}) solid solutions but a-Ti were obtained by W-Ti milled power. This procedure has great advantages in producing nanoroads of complete solid solution powders.

References

1. Benjamin JS (1970) Dispersion strengthened superalloys by mechanical alloying. Metall Trans 1: 2943-51.

2. Benjamin JS, Volin TE (1974) The mechanism of mechanical alloying. Metall Trans 5: 1929-34.

3. Mousavi T, Karimzadeh F, Abbasi MH (2008) Synthesis and characterization of nanocrystalline NiTi intermetallic by mechanical alloying. Mat Sci Eng: A 487: 46-51.

4. Rojas P, Ordonez S, Serafini D, Zuniga A, Lavernia E (2005) Microstructural evolution during mechanical alloying of Mg and Ni. Alloys Compd 391: 267-76.

5. Martinez VP, Aguilar C, Marin J, Ordonez S, Castro F (2007) Mechanical alloying of Cu-Mo powder mixtures and thermodynamic study of solubility Mat Lett 61: 929-33.

6. Koch C, Cavin O, McKamey C (1983) Preparation of amorphous Ni60Nb40 by mechanical alloying. Appl Phys Lett 43: 1017-9.

7. Alford TL, Chen L, Gadre KS (2003) Stability of silver films on various underlying layers at elevated temperatures. Thin Solid Films 429: 248-54.

8. Suryanarayana C (2004) Mechanical Alloying and Milling. Marcel Dekker, New York, USA.

9. Dirks AG, Wolters RAM, Nellissen AJM (1990) On the microstructure property relationship of W-Ti-(N) diffusion barriers Thin Solid Films 193-4: 201-3.

10. Jalali R, Parhizkar M, Bidadi H, Naghshara H (2020) Correlation between optical, structural and microstructural properties of Ti-W-N thin films. Ceram Int 46: 6454-61.

11. Bhagat S, Han S, LAlfrod T (2006) Tungsten-titanium diffusion barriers for silver metallization. Thin Solid Films 515: 1998-2002.

12. Qingxiang W, Shuhua L, Zhikang F, Xin C (2010) Fabrication of W-20wt.%Ti alloy by pressure less sintering at low temperature. Int J Refract Met H 28: 576-9.

13. Chen C, Qian SF, Wang S (2019) The microstructure and property of W/Ti multilayer composites prepared by spark plasma sintering. Int J Refract Met H 79: 138-44.

14. Wang S, Maluo L, Xiangzan MZ (2016) Microstructure and properties of TiN-reinforced W-Ti alloys prepared by spark plasma sintering. Powder Technol 294: 301-6.

15. Kecskes LJ, Hall BIW (1999) Microstructural effects in hot-explosively-consolidated W-Ti alloys. J Mater Process Technol 94: 247-60.

16. Prasanta KS, Suneel KS, Sarika SK, Loganathan D (2015) Microstructure and sintering behavior of nanostructured W-10-20wt.% Ti alloys synthesized by a soft chemical approach. Int J Refract Met H 51: 282-8.

17. Dai W, Liang S, Luo Y, Yang Q (2015) Effect of W powders characteristics on the Ti-rich phase and properties of W-10wt.% Ti alloy. Int J Refract Met H 50: 240-24.

18. Jiang DY, Ouyang CY, Liu SQ (2016) Mechanical properties of W-Ti alloys from first-principles calculations. Fusion Eng Des 106: 34-9.

19. Callisti M, Tichelaar FD, Polcar T (2018) In situ TEM observations on the structural evolution of a nanocrystalline W-Ti alloy at elevated temperatures. J Alloys Compd 749: 1000-8.